Contribution of miR-221-3p to hyperthermia-induced radiosensitivity and its gene targets

Author: Dominika Martinovičová
Student number: 2691921
Email address: d.martinovicova@amsterdamumc.nl
Date of publication: 2.6.2023
Placement: Department of Pathology, VUmc
Daily supervisor: Drs. Mengfei Xu (m.xu@amsterdamumc.nl)
On-site supervisor: Prof. Dr. R. D. M. Steenbergen (r.steenbergen@amsterdamumc.nl)
Second assessor: Dr. Kirsten Rozemeijer (k.rozemeijer@amsterdamumc.nl)
Bachelor's programme: Bachelor of Biomedical Sciences
EC: 24

Table of contents

ABSTRACT

The standard treatment of locally advanced cervical cancer is chemoradiation which often comes with severe side effects. A well-established alternative is combining radiotherapy with hyperthermia (thermoradiation). Dysregulation of microRNAs (miRNAs) is frequently observed in cancer, and growing evidence suggests their usefulness as predictive biomarkers and therapeutic targets. By post-transcriptionally regulating gene expression, miRNAs can largely affect various cellular pathways. In a previous study, we found that miR-221-3p potentially enhances treatment effects of thermoradiation. To investigate the sensitization potential of miR-221-3p on SiHa cells, we conducted a colony formation assay under both single modality and combination treatments. Seventy-two hours after transfection, cells were plated and treated with irradiation (2Gy) and/or hyperthermia (42°C for 60 mins) or kept in an incubator as treatment control. Colonies were counted 14 days post-treatment. We also predicted and validated mRNA targets with online programs, publicly available datasets and qRT-PCR. Our findings demonstrate that miR-221-3p contributes to a reduction in colony formation upon treatment. qRT-PCR revealed downregulation of 3 genes (RAD51, RB1, SMC1A) in miR-221-3p overexpressed cells. This strongly suggests that miR-221-3p contributes to decreased colony formation upon thermoradiation treatment potentially by inhibiting DNA repair pathways. These results emphasize the potential of future miRNA treatment of cancer.

INTRODUCTION

Cervical cancer

Cervical cancer was found to be the fourth most common cancer affecting women worldwide and to have an estimated incidence of over 600 000 new victims in 2020 (Ferlay et al., 2020).

It is believed that the most dominant cause of cervical cancer is the persistent infection by high-risk human papillomavirus (hrHPV) (Cohen et al., 2019). HPV was found to be responsible for more than 95% of cervical cancers (Cervical cancer, n.d.). It is characterized as sexually transmitted disease and screening studies have found that a large majority of sexually active population encounters HPV at least once at some point of their life (Cervical cancer, n.d.). Fortunately, most of these encounters are naturally resolved by the immune system and more than 90% of the infections are eventually eliminated (Cervical cancer, n.d.). If, however, the infection persists, the chances of cancer development increase.

Cervical cancer is clinically classified into 4 major stages by The International Federation of Gynecology and Obstetrics (FIGO). Staging of cervical cancer allows doctors and specialists to design a treatment strategy that aims to eliminate the tumor in the most effective way (Cervical Cancer Treatment by Stage, 2023). Early-stage cancers up to stage IIA are generally treated by surgical excision or if not applicable by chemo- and/or radiotherapy (RT) (Cervical Cancer Treatment by Stage, 2023). This was shown to be an effective way of treatment resulting in 92% rate in 5-year relative survival (Cervical Cancer Prognosis and Survival Rates, 2023). The number, however, rapidly decreases to 59% when considering the locally advanced cancers involving stages IIB, III, and IVA (Cervical Cancer Prognosis and Survival Rates, 2023). The modulated chemo- and RT treatment involving the external and internal radiation has been shown to be less effective in later cervical cancer stages (Mayadev et al., 2022). Moreover, treatments involving chemotherapy are known to cause severe side effects and relatively high toxicity.

The insufficient treatment response in locally advanced cervical cancers creates demand for the development of more effective therapeutic strategies minimizing the growth of the tumor and improving the survival rate without further exacerbating the adverse toxic side effects.

Radiotherapy

As mentioned in the previous paragraph, RT is considered to be one of the standard therapeutic strategies when it comes to treating cervical cancer. RT is a form of treatment causing the formation of ions and thereby either directly or indirectly inducing cell death (Baskar et al., 2012). Direct effects include lethal damage of DNA, such as single- and double-stranded breaks, leading to cells being incapable of further division (Baskar et al., 2012). The indirect effects constitute the formation of free radicals which, due to their high reactivity, tend to disrupt neighboring structures including DNA and thereby, all the same, hinder the cell's multiplication ability (Baskar et al., 2012).

RT has two means of delivery, external beam radiation and internal radiation (brachytherapy) (Baskar et al., 2012). External beam radiation targets the tumor area from outside with photons, protons or other high-energy particle rays to induce the formation of radicals and/or DNA damage (Baskar et al., 2012). On the other hand, internal radiation provides ionizing radiation from inside by administering the radioactive source straight into the tumor (Baskar et al., 2012). All in all, both strategies aim to reduce cell viability and proliferation (Baskar et al., 2012).

Typically, however, treatment strategies do not have 100% efficiency. Due to this, RT is often coupled to chemotherapy, immunotherapy, surgery or hyperthermia (HT) (Baskar et al., 2012). Depending on the treatment plan and the desired outcome, combined or the so-called modulated therapy can be a very efficient tool in fighting and curing cancer (Baskar et al., 2012).

Hyperthermia

HT is a temporal and local increase in temperature of the tumor-containing part of the body, which can be achieved by electromagnetic or acoustic waves and recently also by introducing nanoparticles into the tumor (Burchardt & Roszak, 2018).

RT alone was shown to be less efficient than its combination with other therapies due to tumor cells becoming resistant to radiation under certain conditions (Burchardt & Roszak, 2018). RT resistance has been found to be mostly associated with the S-phase of the cell cycle, lower pH, and decreased perfusion (Burchardt & Roszak, 2018). Modulation of RT with HT, however, was shown to boost the effects of RT and aid in overcoming the resistance. This is mainly due to improved blood flow in the tumor, resulting in reoxygenation of the tumor microenvironment and activation of the immune system (Burchardt & Roszak, 2018).

Firstly, reoxygenation of the tumor environment leads to activation of the BAX dimerization and increase in oxygen levels (D'Alessio et al., 2005). Both of these changes contribute to cell death by promoting the apoptosis pathway and providing the substrate for free radical formation, respectively (Franckena, 2012). Secondly, HT inhibits the function of DNA repair mechanisms ultimately impeding DNA damage response and repair (Burchardt & Roszak, 2018). Lastly, HT has been found to facilitate stronger immune response via heat shock protein 70 (HSP70) (Burchardt & Roszak, 2018). Temperatures in the range of 40-42°C induce synthesis of HSP70, which are known to activate NK cells and ultimately also recruit and induce cytotoxic T-cell reaction (Burchardt & Roszak, 2018). Moreover, 42°C were found to degrade E6 – an HPV oncoprotein promoting the degradation of p53. Increasing the temperature to 42°C can therefore prevent the formation of E6-p53 complex and thereby allow for p53-mediated apoptosis and cell cycle arrest.

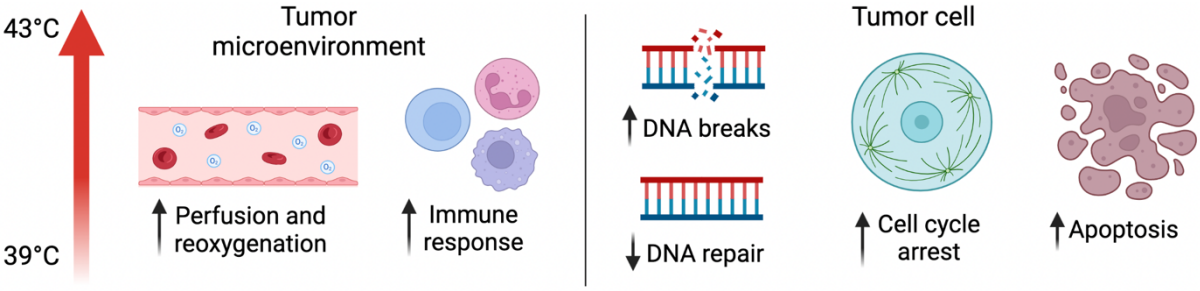

Figure 1.: ***The effects of hyperthermia on tumor cells and their environment.*** *HT increases perfusion resulting in improved oxygenation and enhanced immune response. Additionally, it induces DNA breaks and inhibits DNA repair systems causing cell cycle arrest and apoptosis.*

A systematic review by Lutgens et al. (2009) comprehensively summarized the findings and differences between treatments of locally advanced cervical carcinoma. By looking at the complete tumor response, local tumor recurrence and overall survival, the displayed results clearly showed statistically significant difference and improvement in the RT + HT group compared to only RT (Figure 2.). As for the induction of additional toxicity there seemed to be no difference whatsoever between the two treatment groups both in acute and late toxicity. This was also confirmed by more recent extensive reviews by IJff et al. (2021) and Burchardt and Roszak (2018) which nicely compare the efficiency of RT, chemotherapy, and HT either alone or in various combined treatment strategies in cervical cancer patients. All in all, all these reviews conclude that HT in combination with RT displays additive and, in some cases, even synergistic effects comparable to chemoradiation (Burchardt & Roszak, 2018). Moreover, conversely to chemoradiation, RT + HT has not been associated with any adverse side effects related to toxicity to the organism (Burchardt & Roszak, 2018).

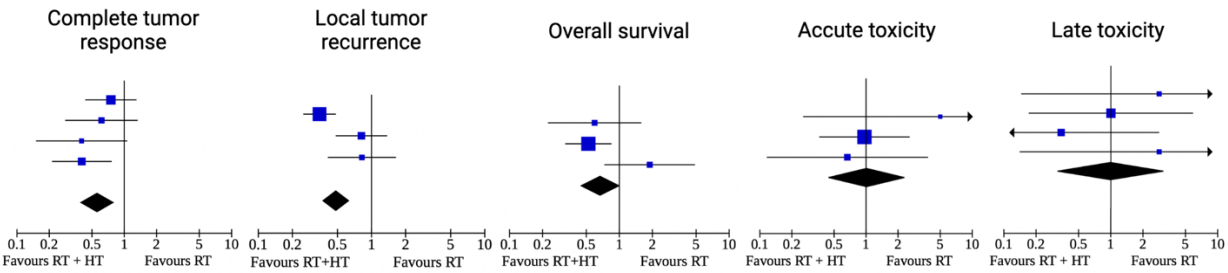

Figure 2.: ***Forest plots from the systematic review article by Lutgens et al. (2010).*** *Statistical analysis of the results from 6 studies included in the review investigating the effect of hyperthermia addition to radiotherapy. All three used endpoints i.e., complete tumor response, local tumor recurrence and overall survival indicate better treatment outcome when hyperthermia was added. Additionally, when looking at toxicity, there was no significant difference discovered.*

miRNA

The main purpose of oncological treatment is to interfere with cellular mechanisms that promote tumorigenesis and thereby stop the cancer growth and spreading. One of the molecules largely involved in regulation of biological processes along with carcinogenesis is microRNA (miRNA). MiRNAs are small non-coding RNA molecules regulating multiple cellular pathways including gene expression, protein translation or mRNA transcription (Peng & Croce, 2016).

MiRNAs are transcribed from non-protein coding regions of the DNA by RNA polymerase II in the form of long primary transcript – pri-miRNA. Pri-miRNA is subsequently cut in the nucleus by a complex of DGCR8 protein and type III RNase Drosha. This step results in precursor miRNA molecule (pre-miRNA), which is 85 nucleotides long and forms a stem-loop structure. After exportin-5 facilitated translocation of the pre-miRNA into the cytoplasm via nuclear pore, RNase III enzyme called Dicer, processes the molecule into a 20-22-nucleotide duplex. Next, the duplex is separated by the AGO2 enzyme into two strands – passenger and mature/guide. Passenger strand is released, and mature strand interacts with the RNA-induced silencing complex, also known as RISC. Mature strand serves as a guide to transport the RISC complex to the target molecule which the miRNA complementarily binds. After miRNA-RISC complex binds the target molecule it can lead to either inhibiting translation or complete degradation of the mRNA (Figure 3.).

Being involved in the post-transcriptional biological processes enables miRNAs to be an important regulator when it comes to future development and behavior of the cell. It is, therefore, crucial for the miRNA levels to be optimal. Considering the large genetic changes and mutations in the genome of tumor cells, it is hardly imaginable that miRNA expression and function would remain unaltered. This has been also experimentally studied and the results show that the levels of miRNA in tumor cells are indeed highly dysregulated, and the observed consequences all contribute to the oncogenic cell properties known as the hallmarks of cancer (Peng & Croce, 2016).

Besides that, miRNAs were also found to sensitize the tumor and facilitate its elimination. Vescarelli et al. found that miR-200c can sensitize ovarian cancer cells and make them more vulnerable to PARP1-inhibitor (Vescarelli et al., 2020). MiR-21-3p was identified as a sensitizing agent in melanoma and miR-124-3p was found to sensitize hepatocellular carcinoma cells to therapy (Dong et al., 2022; Guo et al., 2022). These examples illustrate the potential of miRNA in cancer treatment.

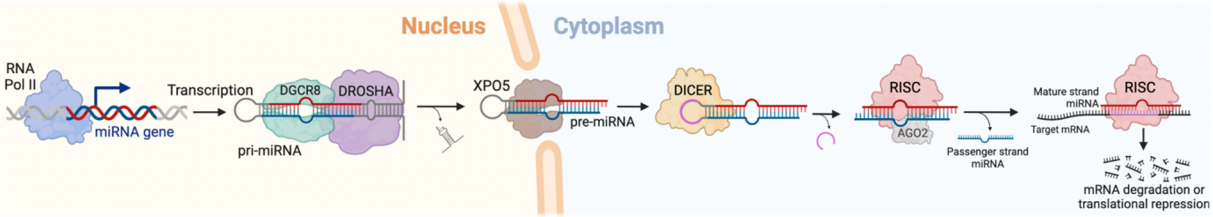

Figure 3.: ***MiRNA biogenesis.*** *After RNA polymerase II guided transcription, is the transcribed pri-miRNA molecule cleaved by DGCR8-DROSHA protein complex forming the pre-miRNA. Pre-miRNA is then transported by XPO5 via nuclear pore into the cytoplasm. Subsequently, it is cleaved by RNase Dicer and the remaining double strand is separated by Ago2 protein. Finally, mature or guide miRNA strand incorporates itself into the RISC complex and guides it to target molecules.*

Therapeutic potential

The dysregulation of miRNA in cancer and its multi-targeting property makes it a potential therapeutic molecule for treatment response. The combination of standard RT with HT treatment modulation and miRNA sensitization could lead to an optimized therapeutic strategy used to eliminate tumors in cancer patients (Figure 4.). In order to utilize the full therapeutic potential of miRNAs in cervical cancer, it is first necessary to recognize and validate possible miRNA candidates involved in sensitization of the tumor cells and secondly identify their target genes to better understand the underlying mechanism. By screening approximately 380 miRNAs on 4 cervical cancer cell lines (SiHa, HeLa, CaSki, C4-I) 55 miRNAs were identified as potential sensitizers of thermoradiation. In this research, we aimed to further look into the effect of miR-221-3p overexpression on single modality and combined treatment by performing colony formation assay of transfected SiHa cell lines subjected to (thermo)radiotherapy treatment. After validation, miR-221-3p will be investigated for its biological relevance by predicting and verifying its mRNA targets using online tools and qRT-PCR.

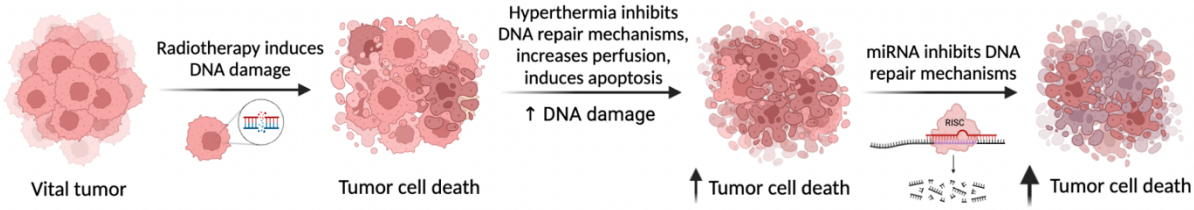

Figure 4.: ***Combined radiotherapy with hyperthermia sensitization and miRNA interference****. Upon radiation exposure, tumor cells acquire DNA damage which predisposes them to cell death. By adding hyperthermia to treatment, cells become more sensitive to radiotherapy due to decreased functionality of DNA repair mechanisms and changes in tumor microenvironment. Finally, we hypothesize that the addition of certain miRNA could optimize this treatment even further by hampering the translation of proteins involved in DNA repair.*

METHODS

Cell culture

Human cervical cancer cell line, SiHa, was grown in Dulbecco's Modified Eagle Medium (DMEM, 4.5g/L D-glucose, L-glutamine; Thermo Fisher Scientific, San Jose, CA, USA) supplemented with 10% fetal bovine serum (FBS; Thermo Fisher Scientific), penicillin (12 000 units/mL), streptomycin (10 000 µg/mL) and L-glutamine (29.2mg/mL) (Thermo Fisher Scientific). Cell lines were retrieved from American Type Culture Collection (ATCC, Manassas, VA, USA) and verified by STR testing (Babion et al., 2020). All cultures were grown in 10ml of the complete medium described above in a 10cm diameter Petri dish and kept in an incubator at 37 °C in a humified atmosphere of 5% CO_2.

Transfection with miRNA mimics

SiHa cells were transfected with a final concentration of 2nM miR-221-3p mimic (C-300578-05-0002; GE HealthCare Technologies, Chicago, Illinois), siPLK1 (Horizon Discovery, Cambridge, UK), or negative control #2 (1527170; Horizon Discovery, Cambridge, UK) mixed with 2µL/well of DharmaFECT 4 (Horizon Discovery) and seeded 85 000 cells/well in 6-well plate. The end volume of cell suspension together with transfection mix was 2mL in each well. The transfected cells were incubated for 3 days at 37°C in a humidified atmosphere of 5% CO_2 before harvesting for colony formation assay and RNA isolation.

Colony formation assay

Cell distribution

To find the optimal way of cell plating, 5 different techniques were tested:

1. Adding only 1 ml of liquid, containing the desired number of cells, and letting the cells sink to the bottom for 1 hour before adding the remaining 2 ml of medium.
2. Firstly, adding the necessary volume of medium and then the cell suspension resulting in 3 ml of complete working volume.
3. Addition of the cell suspension and medium while tilting the 6-well plate under 45° and then placing the plate on the table and letting the liquid cover the bottom of the well.
4. Preparation of master mix for each concentration and adding 2 ml of the mixture at once.
5. First adding cell suspension with the desired number of cells and subsequently adding medium to result in a final volume of 3 ml.

Cell survival

The cells were distributed to multiple 6-well plates ranging from 50 to 2000 cells per well according to the following scheme 3 days post transfection (Figure 5.). The plated cells were then left to sink to the bottom of the plate for 1 hour at room temperature before transferring them to the incubator for another 3-4 hours (37 °C, 5% CO_2). Next, each of the 6-well plates was treated with irradiation (2Gy) and/or HT (42°C, 60 mins), or kept cultured as control. The time interval between irradiation and hyperthermia was less than 30 mins. Following the treatment, the cells were incubated for 10-14 days before fixing and staining with crystal violet (5mg/ml crystal violet in 10% ethanol, 50% methanol and 40% water). The plates were scanned and counted with Oxford Optronics GelCount (v1.1.2.0; Oxford Optronics).

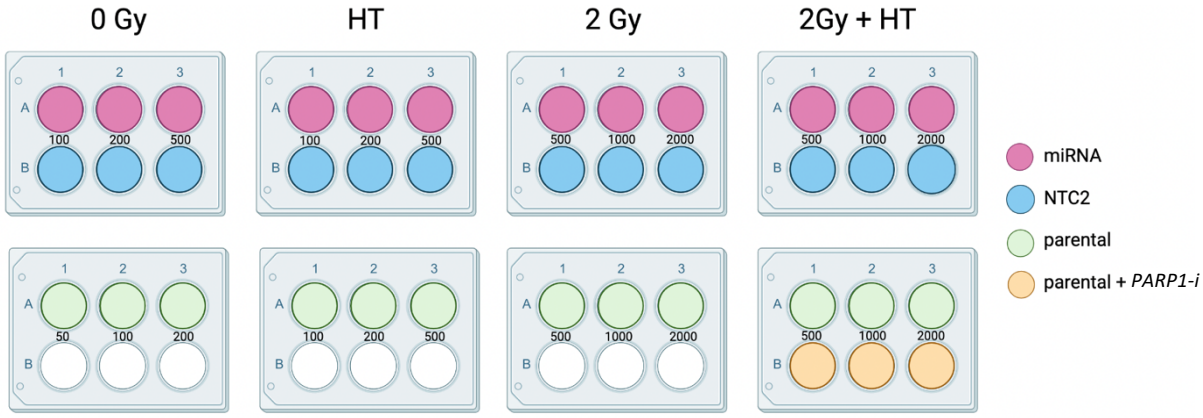

Figure 5.: ***Colony formation assays plating and treatment scheme.*** *Transfected and parental cells were seeded in different density to 6-well plates and subjected to different conditions. The numbers ranging from 50 to 2000 marked between the wells indicate the number of cells plated in the corresponding wells. Additionally, in the last 6-well plate, PARP-1 inhibitor was added to parental cells with the intention to serve as a positive control for treatment enhancement. Gy – gray (irradiation unit); HT – hyperthermia (42°C, 60 mins); NTC2 – negative control, PARP1-i – poly (ADP-ribose) polymerase 1 inhibitor*

miRNA target prediction

Target prediction of miR-221-3p was carried out using The Encyclopedia of RNA Interactomes (ENCORI) platform (https://starbase.sysu.edu.cn/) (J. H. Li et al., 2014). It uses the StarBase v3.0 database integrating data from 7 different RNA databases and capable of finding complementary regions between miRNA seed sequence and 3'untranslated region of mRNA (J. H. Li et al., 2014).

Next, wikipathways enrichment of predicted targets was performed using The Database for Annotation, Visualization and Integrated Discovery (DAVID) Bioinformatics Database (https://david.ncifcrf.gov/home.jsp) (Sherman et al., 2022).

Finally, the expression profile of miR-221-3p was obtained from The Cancer Genome Atlas (TCGA) cervical cancer cohort and the National Center for Biotechnology Information (NCBI) Gene Expression Omnibus (GEO) DataSets number GSE30656 (Wilting et al., 2013). mRNA expression of potential target genes from cervical cancer tissues were also obtained from TCGA and GSE138080 (Babion et al., 2020). Due to lack of certain tissue samples in the mRNA dataset, only the samples present in both datasets were used for further analysis. Therefore, all the adenocarcinoma and 3 of the CIN samples were excluded resulting in 35 samples.

Negative correlation coefficient of the co-expression of miRNA-221-3p and mRNA of interest was set as criterion for further selection and analysis.

RNA isolation and quantitative reverse transcription-polymerase chain reaction (qRT-PCR)

RNA isolation

The total RNA was isolated following the QIAGEN RNeasy Protocol: Purification of Total RNA from Animal Cells Using Spin Technology. The collected SiHa cells were first lysed by 600µL Buffer RLT (QIAGEN®, Venlo, The Netherlands) and homogenized using a 20-gauge syringe. Subsequently, 70% ethanol was added to the cell lysate and the mixture was centrifuged through a spin column for 30s at 10 000rpm. Next, the column was washed and centrifuged with Buffer RW1 (QIAGEN; 30s, 10 000rpm) after which the lysates were treated with 7% DNase treatment mix (RQ1 (Promega, Leiden, The Netherlands) mixed in Buffer RDD (QIAGEN)) and incubated at room temperature for 30min. Following the DNase treatment, the column was washed with 350µL Buffer RW1 (QIAGEN) and centrifuged (30s, 10 000rpm). To thoroughly wash the membrane-bound RNA, the column was washed twice with 5x-diluted Buffer RPE (QIAGEN) in 100% ethanol (30s, 10 000rpm) and subsequently centrifuged (2min, 10 000rpm) with nothing added, to rid the sample of any remaining buffers or compounds.

Lastly, after the addition of 30µL RNase-free water (QIAGEN), the RNA was collected by centrifugation (1min, 10 000rpm) into a 1.5mL Eppendorf tube. Concentration was measured using NanoDrop Microvolume UV-Vis Spectrophotometer (Thermo Fisher Scientific) and stored in -80°C.

miRNA levels

MiRNA levels in the isolated RNA samples were subjected to reverse transcription reaction. This was performed using the TaqMan MicroRNA Reverse Transcription Kit (Thermo Fisher Scientific).

From each sample 5ng of RNA was added to a reverse transcription master mix containing 10x RT buffer, dNTPs with dTTP (100mM), RNase inhibitor (20U/µL), MultiScribe reverse transcription enzyme (50U/µL), water, and primers for miR-221-3p and reference small nucleolar RNA (U75). After the samples were incubated on ice for 5min, a reverse transcription reaction was performed in three steps. Firstly, the samples were kept at 16°C for 30 mins. Secondly, the temperature was increased to 42°C for 30 mins. And lastly, the samples were incubated at 85°C for 5 mins.

Quantification of the obtained cDNA was performed using the TaqMan assay for miR-221-3p and U75, water and TaqMan Universal Master Mix II (no UNG) (Thermo Fisher Scientific). The PCR program was set to initial 10 mins at 95°C followed by 45 cycles of 15s at 95°C and 1 min at 60°C.

Primer design

The predicted target genes were searched in the Ensemble Genome Browser (https://www.ensembl.org/index.html) in order to obtain their GenBankID and exon junction positions. Next, using the PrimerQuest™ Tool on Integrated DNA Technologies website (https://eu.idtdna.com/pages), we designed primers with the following properties – optimal T_m: 60°C, optimal GC content: 50%, optimal size: 22 bp. The amplicon size was set between 100 and 150 bp. Out of the generated primer assays, we selected the ones with around 50% GC content and preferably the ones spanning the exon junctions (Appendix, Table 4.). This ensured primer stability and minimized amplification of target sequences originating from gDNA. Specificity of primers was checked with BLAST. The obtained information was subsequently used to annotate the exons and add primers to the predicted target mRNAs using the SnapGene software (www.snapgene.com).

mRNA expression

mRNA present in the purified RNA samples was first reverse transcribed using the iScript cDNA Synthesis Kit and protocol (Bio-Rad, California, USA). Reaction mix was combined with purified RNA sample with final concentration of 20% 5x iScript Reaction Mix, 5% iScript Reverse Transcriptase, 25% Nuclease-free water and 25ng/µL RNA purified sample. Subsequently, the samples were incubated for 5min at 25°C, followed by 30min at 42°C and 5min at 85°C. Finally, the samples were diluted with water in a ratio 1:1 to end concentration of 12.5ng/µL of RNA.

Following reverse transcription, Fast SYBR Green Master Mix and the associated protocol for real-time - qPCR (Thermo Fisher Scientific) were used and pursued. The final reaction mix consisted of 2µL of cDNA, 5µL of the 2x SYBR Green PCR Master Mix, 0.5µM of forward and reverse primers and 2.5µL water. Next, the sample was subjected to a PCR reaction with initial 20s at 95°C followed by 4 cycles of 3s at 95°C and 30s at 60°C. The PCR reaction was performed using the Applied Biosystems™ 7500 Fast Dx Real-Time PCR Instrument (Thermo Fisher Scientific).

Statistical analysis

Survival fraction (SF) was calculated using the formula *(number of survived cells/number of seeded cells)/plating efficiency* with plating efficiency being the fraction of NTC2-transfected cells that survived under 0Gy condition. All the SF calculations were performed in Microsoft Excel and significance was calculated using unpaired t-test in GraphPad Prism 9.

Potential mRNA targets were predicted using ENCORI and DAVID online databases. Spearman's correlation coefficient between miR-221-3p and the respective targets was calculated in Matlab_r2022b (Appendix, Code 1.).

MiR-221-3p levels in miR-221-3p-transfected cells and NTC2-transfected cells were normalized to the expression of small nucleolar RNA U75 by calculating the difference between Ct values and the expression was calculated as $2^{-\Delta Ct}$ in Microsoft Excel. Statistical significance was calculated using unpaired t-test in GraphPad Prism 9. mRNA expression was normalized to housekeeping genes RPLP0 and BGUS and fold change for miR-221-3p overexpressed cells with regards to NTC2-transfected cells was calculated as $2^{-\Delta\Delta Ct}$ in Microsoft Excel (Livak & Schmittgen, 2001). Statistical significance was calculated in GraphPad Prism 9 using an unpaired t-test.

RESULTS

Colony formation assay

Cell distribution

In order to analyze the results from the colony formation assays, it is necessary for the colonies to be equally distributed in the wells to get separate and distinguishable colonies. Using the master mix, 45 degrees tilting and addition of medium before adding cell suspension, all resulted in gathering of the cells in the middle of the well. This is undesirable due to inability to distinguish individual cell colonies. Next, adding only 1mL of the cell suspension at first, resulted in a ring of cells close to the edge of well, most probably as a consequence of the capillary action. The best distribution technique turned out to be initial addition of desired cell number in cell suspension and only after that addition of medium to match the final volume of 3mL (Figure 6.).

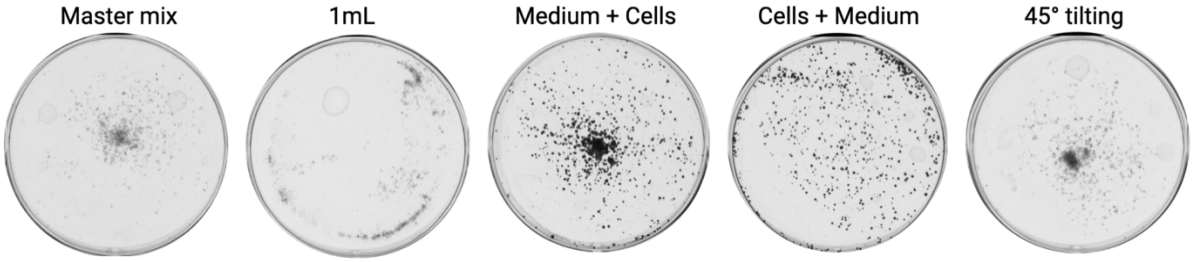

Figure 6.: ***Cell distribution strategies****. Master mix, medium + cells and 45° tilting resulted in the accumulation of cells in the center of the well. Initial addition of 1mL only, lead to a ring-like formation of the cells. Lastly, adding cells before the medium yielded the best distribution, equally spreading the cells across the whole bottom of the well.*

miR-221-3p adds to hyperthermia-induced radiosensitivity

In order to compare the survival fraction between miRNA-transfected and NTC2-transfected SiHa cells, colony formation assay was performed. Since transfection itself causes stress and thereby contributes to decreased cell survival, plating efficiency was calculated with 0Gy NTC2-transfected cells. Based on plating efficiency, survival fraction of all treatment condition was calculated.

MiR-221-3p exhibits a stable statistically significant trend of reducing colony formation of SiHa cells in all 4 conditions (Figure 7.). Under control 0Gy condition miR-221-3p-transfected SiHa cells show significantly decreased survival ($mean_{miR\text{-}221\text{-}3p\ overexpressed\ cells} = 0.2$, $mean_{NTC2\text{-}transfected\ cells} = 1$, $p = 0.0034$). This holds true for the sole exposure to HT as well as 2Gy ($mean_{miR\text{-}221\text{-}3p\ overexpressed\ cells} = 0.13$, $mean_{NTC2\text{-}transfected\ cells} = 0.55$, $p = 0.0013$; $mean_{miR\text{-}221\text{-}3p\ overexpressed\ cells} = 0.12$, $mean_{NTC2\text{-}transfected\ cells} = 0.71$, $p = 0.0021$). And lastly, under the modulated treatment conditions of RT with HT the difference in survival was also shown to be significantly lower for the miR-221-3p-transfected SiHa cells ($mean_{miR\text{-}221\text{-}3p\ overexpressed\ cells} = 0.035$, $mean_{NTC2\text{-}transfected\ cells} = 0.24$, $p = 0.0027$) (Figure 7.).

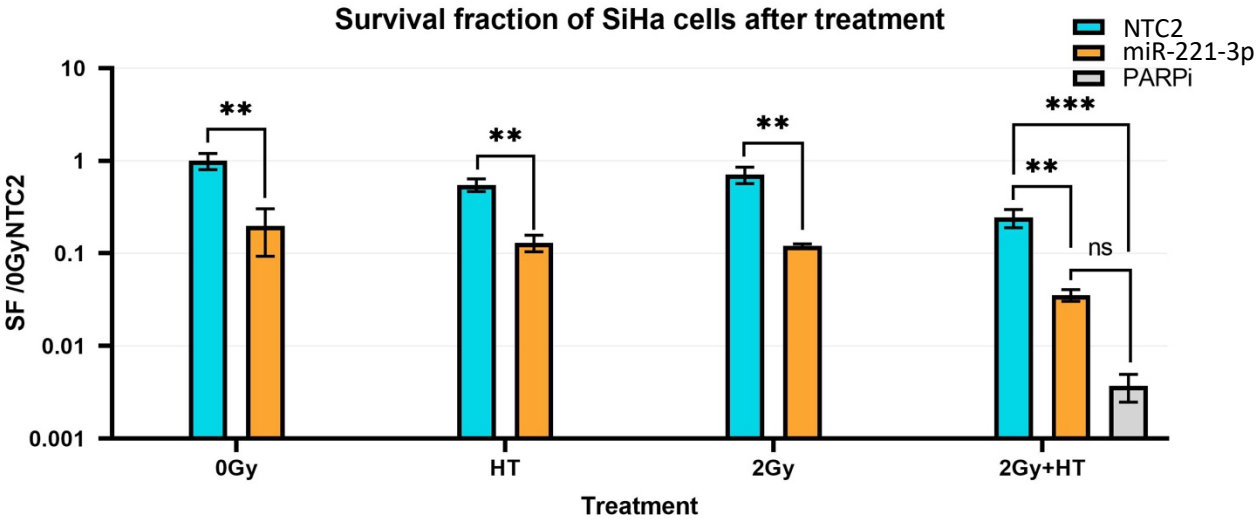

Figure 7.: ***Survival fraction of SiHa cells after treatment.*** *All samples were standardized with respect to 0Gy NTC2-transfected SiHa cells. There is a significant difference in survival between NTC2- and miR-221-3p-transfected SiHa cells under all 4 treatment conditions. The error bars indicate SD. (ns – not significant, ** - p < 0.01, *** - p < 0.001)*

Target prediction

Using ENCORI online platform, 2 923 potential gene targets were identified for miR-221-3p. This gene list was subsequently used as the input information for DAVID gene enrichment analysis and only the genes involved in pathways related to DNA damage and repair found by wikipathways were chosen for further investigation. Wikipathways analysis listed 6 pathways relevant for DNA damage repair - ATM signaling, DNA damage response, DNA damage response (only ATM dependent), DNA irradiation damage and cellular response via ATM, DNA irradiation double stranded break and cellular response via ATM, miRNA regulation of DNA damage response (Appendix, Table 1.). Altogether 64 genes were found to be involved in at least one of these pathways (Appendix, Table 2.).

Next, using Matlab_r2022b and the data present in TCGA and in-house datasets, we calculated the correlation coefficient between the miR-221-3p and the 64 genes of interest. Out of the 64 genes, 26 were found to be negatively correlated in both the in-house and TCGA datasets (Appendix, Table 3.). Lastly, considering the HITS-CLIP (HC) data, the genes with the highest HC ranking were CDKN1B, BCL2L11, MDM2, CCND1, SMC1A, ATF2, TOPBP1, RB1 and UPF1. Two additional genes, FOXO3 and RAD51, were included in the analysis due to their critical role in DNA damage repair (Liu et al., 2018) (Chen et al., 2017).

miRNA/mRNA expression

To investigate the effect of miR-221-3p on the levels of predicted target mRNA/genes, qRT-PCR was performed on the cDNA samples. Firstly, miR-221-3p overexpression were confirmed in miR-221-3p transfected cells ($cmean_{\text{miR-221-3p overexpressed cells}} = 2.615$, $mean_{\text{NTC2-transfected cells}} = 0.17$, $p = 0.0021$) (Figure 8. A).

Secondly, the fold change of the expression of candidate targets in miR-221-3p overexpressed cells was calculated with respect to the NTC2-transfected cells (Figure 8. B). Seven genes (ATF2, CDKN1B, MDM4, RAD51, TOPBP1, RB1, SMC1A) were found below FC = 1, out of which three (RAD51, RB1, SMC1A) were found below the threshold FC = 0.7 in miR-221-3p-transfected SiHa. Lastly, five mRNAs (BCL2L11, CCND1, FOXO3, MDM2, UPF1) were found above the FC = 1 threshold.

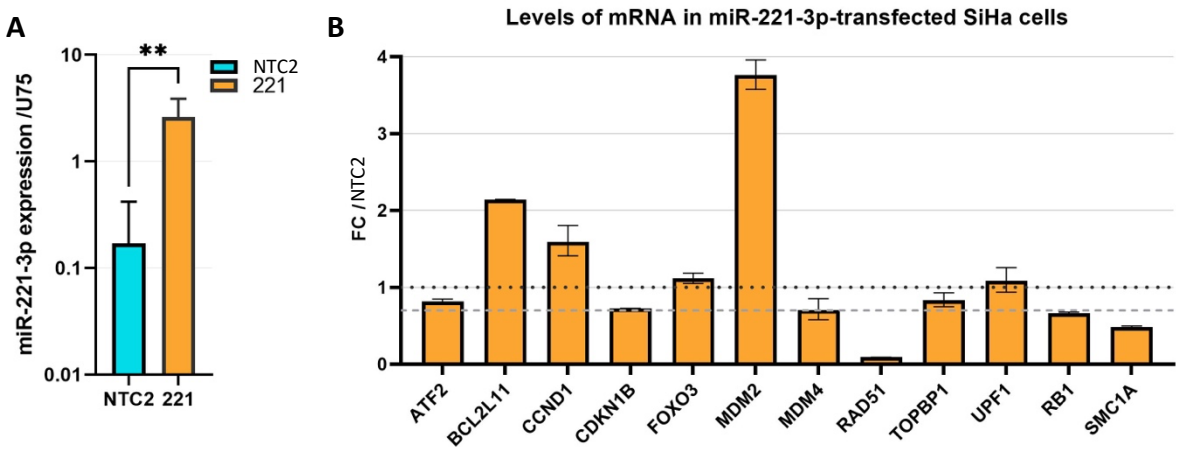

Figure 8.: ***miRNA/mRNA levels and expression in NTC2- and miR-221-3p-transfected SiHa cells.*** *(A) MiR-221-3p levels normalized with respect to reference small nucleolar RNA U75. MiR-221-3p-transfected cells show significantly higher levels of miR-221-3p. (B) Fold change of mRNA levels in miR-221-3p-overexpressed SiHa cells with respect to NTC2-transfected SiHa cells. dotted line – FC = 1, the levels of the respective mRNA the same as in control sample; dashed line – FC = 0.7, the levels of the respective mRNA are 30% lower than in control sample; ** - $p < 0.01$*

DISCUSSION

The focus of this study was firstly to investigate the treatment effect of hyperthermia, irradiation and thermoradiation upon miR-221-3p overexpression and secondly to predict and identify its mRNA targets.

The survival fraction was evaluated by performing colony formation assay and showed a clear trend that miR-221-3p overexpression contributes to therapeutic effect under all 4 tested conditions including the radiotherapy modulated with hyperthermia treatment. This is in line with preceding exploratory screening which identified miR-221-3p as one of the potential sensitizing miRNAs.

Moreover, a research group Shi et al. (2021) found decrease in DNA double stranded breaks upon miR-221-3p inhibition which supports our hypothesis that overexpression of miR-221-3p has the opposite effect and contributes to higher rate of apoptosis eventually leading to increased cell death (Shi et al., 2021). These findings suggest that miR-221-3p is either directly or indirectly affecting pathways relevant for DNA damage repair.

In order to better understand the working mechanism of miR-221-3p-induced decrease of SiHa cells survival, it is necessary to first identify mRNAs targeted by this miRNA. As RT disrupts DNA integrity and we observed decreased survival fraction upon miR-221-3p-transfection, we predicted the mRNA targets to be involved in DNA damage repair pathways. Besides computational prediction based on matching sequence to miR-221-3p we also considered HITS-CLIP score, which represents the number of experimental studies finding a binding site for Ago2 protein which is part of the RISC complex. This information supports our prediction as mRNAs with higher HITS-CLIP score have a higher chance of true interaction with miR-221-3p. Negatively correlated targets with the highest HITS-CLIP values were further examined by qRT-PCR.

By performing qRT-PCR of the predicted targets we found a downregulation below FC = 0.7 of the following genes: RAD51, RB1, and SMC1A in miR-221-3p-overexpressed SiHa cells compared to NTC2-transfected SiHa cells. The complexity of cellular pathways and considerable number of miRNA targets make it challenging to generalize the effect of miRNA on carcinogenesis. Nevertheless, the effects of these genes with regards to cancer and DNA damage from previous studies are worth mentioning as this can spark ideas for future investigation.

RAD51 is one of the crucial enzymes in DNA double-stranded break repair (Wright et al., 2018). In a study by Chen et al. (2017), RAD51 was found to be upregulated in squamous cervical cancer and to be a promoting factor in cell cycle progression. Additionally, this upregulation is thought to contribute to chemo- and radiotherapy as it facilitates DNA damage repair (Demeyer et al., 2021). Inhibition of RAD51 could therefore potentially enhance cancer treatment.

Similarly, RB1 is also known to have a major role in the repair of double-stranded breaks as it facilitates the joining of loose DNA ends. The suppression of RB was found to negatively affect DNA stability upon irradiation and thereby to contribute to chromosomal mutations (Huang et al., 2016).

SMC1A has so far been reported to be involved mostly in cases of colorectal cancer, in which it was found to promote cell cycle progression (J. Li et al., 2016). Moreover, similarly as with the previously mentioned genes, silencing of SMC1A attenuated cell cycle, induced apoptosis and significantly decreased the growth of tumors in mice models (Wang et al., 2015).

Altogether, all the genes mentioned above are reported to contribute to tumor proliferation and their silencing was found to improve the prognosis of cancer. Based on our results, however, we can only conclude that these genes were found to be downregulated upon miR-221-3p overexpression. Further research should therefore focus on identifying and validating the targets of this particular miRNA and gradually uncover the axis describing cell sensitization upon miR-221-3p transfection followed by treatment.

Our study is one of many that highlight that even molecules as small as miRNAs have the potential to largely influence cell's wellbeing and survival. With cancer remaining one of the top causes of death, novel effective types of treatment are necessary to combat this disease. And even though further research is needed, we believe that miRNAs have the potential to alter cancer prognosis and possibly become part of cancer treatment.

CONCLUSION

In summary, miR-221-3p was found to contribute to hyperthermia-induced radiosensitivity by performing colony formation assay with SiHa cells as a model for cervical cancer. With online target prediction program, we identified 26 candidate targets. Subsequently, using qRT-PCR we observed downregulation of RAD51, RB1, and SMC1A genes, indicating either direct or indirect interference of miR-221-3p with the respective mRNAs. The results of this study suggest that miR-221-3p affects cell survival potentially by inhibiting DNA damage repair pathways and therefore should be taken into consideration when developing novel cancer treatments.

ACKNOWLEDGEMENTS

I would like to express my gratitude to Drs. M. Xu and Prof. Dr. R.D.M. Steenbergen for supervising my bachelor's project, supporting my internship, and enabling me to expand on my research experience both as a member of a scientific community as well as on learning new skills in laboratory environment. I would like to especially thank Drs. M. Xu for her endless support and guidance throughout my internship, thanks to which I gained valuable experience that I will benefit from in the future.

REFERENCES

Articles

Babion, I., Jaspers, A., van Splunter, A. P., van der Hoorn, I. A. E., Wilting, S. M., & Steenbergen, R. D. M. (2020). MiR-9-5p exerts a dual role in cervical cancer and targets transcription factor TWIST1. *Cells*, *9*(1). https://doi.org/10.3390/cells9010065

Baskar, R., Lee, K. A., Yeo, R., & Yeoh, K. W. (2012). Cancer and radiation therapy: Current advances and future directions. In *International Journal of Medical Sciences* (Vol. 9, Issue 3, pp. 193–199). https://doi.org/10.7150/ijms.3635

Burchardt, E., & Roszak, A. (2018). Hyperthermia in cervical cancer – current status. In *Reports of Practical Oncology and Radiotherapy* (Vol. 23, Issue 6, pp. 595–603). Urban and Partner. https://doi.org/10.1016/j.rpor.2018.05.006

Chen, Q., Cai, D., Li, M., & Wu, X. (2017). The homologous recombination protein RAD51 is a promising therapeutic target for cervical carcinoma. *Oncology Reports*, *38*(2), 767–774. https://doi.org/10.3892/or.2017.5724

Cohen, P. A., Jhingran, A., Oaknin, A., & Denny, L. (2019). Cervical cancer. In *www.thelancet.com* (Vol. 393). http://clinicaltrials.gov,

D'Alessio, M., de Nicola, M., Coppola, S., Gualandi, G., Pugliese, L., Cerella, C., Cristofanon, S., Civitareale, P., Ciriolo, M. R., Bergamaschi, A., Magrini, A., & Ghibelli, L. (2005). Oxidative Bax dimerization promotes its translocation to mitochondria independently of apoptosis. *The FASEB Journal*, *19*(11), 1504–1506. https://doi.org/10.1096/fj.04-3329fje

Demeyer, A., Benhelli-Mokrani, H., Chénais, B., Weigel, P., & Fleury, F. (2021). Inhibiting homologous recombination by targeting RAD51 protein. In *Biochimica et Biophysica Acta - Reviews on Cancer* (Vol. 1876, Issue 2). Elsevier B.V. https://doi.org/10.1016/j.bbcan.2021.188597

Dong, Z. bin, Wu, H. miao, He, Y. cheng, Huang, Z. ting, Weng, Y. hui, Li, H., Liang, C., Yu, W. ming, & Chen, W. (2022). MiRNA-124-3p.1 sensitizes hepatocellular carcinoma cells to sorafenib by regulating FOXO3a by targeting AKT2 and SIRT1. *Cell Death and Disease*, *13*(1). https://doi.org/10.1038/s41419-021-04491-0

Franckena, M. (2012). Review of radiotherapy and hyperthermia in primary cervical cancer. In *International Journal of Hyperthermia* (Vol. 28, Issue 6, pp. 543–548). https://doi.org/10.3109/02656736.2012.670835

Huang, P. H., Cook, R., Zoumpoulidou, G., Luczynski, M. T., & Mittnacht, S. (2016). Retinoblastoma family proteins: New players in DNA repair by non-homologous end-joining. *Molecular and Cellular Oncology*, *3*(2). https://doi.org/10.1080/23723556.2015.1053596

Li, J., Feng, W., Chen, L., & He, J. (2016). Downregulation of SMC1A inhibits growth and increases apoptosis and chemosensitivity of colorectal cancer cells. *Journal of International Medical Research*, *44*(1), 67–74. https://doi.org/10.1177/0300060515600188

Li, J. H., Liu, S., Zhou, H., Qu, L. H., & Yang, J. H. (2014). StarBase v2.0: Decoding miRNA-ceRNA, miRNA-ncRNA and protein-RNA interaction networks from large-scale CLIP-Seq data. *Nucleic Acids Research*, *42*(D1). https://doi.org/10.1093/nar/gkt1248

Liu, Y., Ao, X., Ding, W., Ponnusamy, M., Wu, W., Hao, X., Yu, W., Wang, Y., Li, P., & Wang, J. (2018). Critical role of FOXO3a in carcinogenesis. In *Molecular Cancer* (Vol. 17, Issue 1). BioMed Central Ltd. https://doi.org/10.1186/s12943-018-0856-3

Livak, K. J., & Schmittgen, T. D. (2001). Analysis of relative gene expression data using real-time quantitative PCR and the 2-ΔΔCT method. *Methods*, *25*(4), 402–408. https://doi.org/10.1006/meth.2001.1262

Mayadev, J. S., Ke, G., Mahantshetty, U., Pereira, M. D., Tarnawski, R., & Toita, T. (2022). Global challenges of radiotherapy for the treatment of locally advanced cervical cancer. In *International Journal of Gynecological Cancer* (Vol. 32, Issue 3, pp. 436–445). BMJ Publishing Group. https://doi.org/10.1136/ijgc-2021-003001

Peng, Y., & Croce, C. M. (2016). The role of microRNAs in human cancer. In *Signal Transduction and Targeted Therapy* (Vol. 1). Springer Nature. https://doi.org/10.1038/sigtrans.2015.4

Sherman, B. T., Hao, M., Qiu, J., Jiao, X., Baseler, M. W., Lane, H. C., Imamichi, T., & Chang, W. (2022). DAVID: a web server for functional enrichment analysis and functional annotation of gene lists (2021 update). *Nucleic Acids Research*, *50*(W1), W216–W221. https://doi.org/10.1093/nar/gkac194

Shi, L., Feng, L., Tong, Y., Jia, J., Li, T., Wang, J., Jiang, Z., Yu, M., Xia, H., Jin, Q., Jiang, X., Cheng, Y., Ju, L., Liu, J., Zhang, Q., & Lou, J. (2021). Genome wide profiling of miRNAs relevant to the DNA damage response induced by hexavalent chromium exposure (DDR-related miRNAs in response to Cr (VI) exposure). *Environment International*, *157*. https://doi.org/10.1016/j.envint.2021.106782

Vescarelli, E., Gerini, G., Megiorni, F., Anastasiadou, E., Pontecorvi, P., Solito, L., de Vitis, C., Camero, S., Marchetti, C., Mancini, R., Benedetti Panici, P., Dominici, C., Romano, F., Angeloni, A., Marchese, C., & Ceccarelli, S. (2020). MiR-200c sensitizes Olaparib-resistant ovarian cancer cells by targeting Neuropilin 1. *Journal of Experimental and Clinical Cancer Research*, *39*(1). https://doi.org/10.1186/s13046-019-1490-7

Wang, J., Yu, S., Cui, L., Wang, W., Li, J., Wang, K., & Lao, X. (2015). Role of SMC1A overexpression as a predictor of poor prognosis in late stage colorectal cancer. *BMC Cancer*, *15*(1). https://doi.org/10.1186/s12885-015-1085-4

Wright, W. D., Shah, S. S., & Heyer, W. D. (2018). Homologous recombination and the repair of DNA double-strand breaks. In *Journal of Biological Chemistry* (Vol. 293, Issue 27, pp. 10524–10535). American Society for Biochemistry and Molecular Biology Inc. https://doi.org/10.1074/jbc.TM118.000372

Websites

Cancer (no date) *World Health Organization*. https://www.who.int/news-room/fact-sheets/detail/cancer (Accessed: February 14, 2023)

Cervical cancer (no date) *World Health Organization*. https://www.who.int/news-room/fact-sheets/detail/cervical-cancer (Accessed: February 14, 2023)

Cervical Cancer Treatment by Stage. *National Cancer Institute.* https://www.cancer.gov/types/cervical/treatment/by-stage (Accessed: March 3, 2023)

Cervical Cancer Prognosis and Survival Rates. *National Cancer Institute.* https://www.cancer.gov/types/cervical/survival (Accessed: March 3, 2023)

Ferlay J, Ervik M, Lam F, Colombet M, Mery L, Piñeros M, Znaor A, Soerjomataram I, Bray F (2020). Global Cancer Observatory: Cancer Today. Lyon, France: International Agency for Research on Cancer. Available from: https://gco.iarc.fr/today, accessed [11.4.2023].

Roser, M., & Ritchie, H. (2015, July 3). *Cancer*. Our World in Data. Retrieved February 11, 2023, from https://ourworldindata.org/cancer#cancer-is-one-of-the-leading-causes-of-death).

APPENDICES

Table 1.: **Pathways related to DNA damage and repair.**

Term	Count	%	PValue	Genes	List Total	Pop Hits	Pop Total	Fold Enrichment	Bonferroni	Benjamini	FDR
WP707~DNA damage response	27	0,850	4,8E+10	RB1, CDKN1B, MRE11, BRCA1, BBC3, CCND3, CCND2, CCND1, CASP3, ABL1, NBN, APAF1, TNFRSF10B, SMC1A, PML, RAD50, RAD51, CREB1, CDK6, RRM2B, FANCD2, CDK2, CDK1, MDM2, CYCS, ATM, RAD1	1430	69	8200	2,2438E+16	0,034	0,004	0,004
WP2516~ATM signaling pathway	16	0,503	0,00198	ATF2, MRE11, BRCA1, SMC1A, AP3B2, RAD50, RAD51, CREB1, FANCD2, CDK2, MDM2, CDK1, ABL1, MDM4, ATM, NBN	1430	40	8200	2,2937E+16	0,758	0,046	0,043
WP3959~DNA IR-double strand breaks and cellular response via ATM	18	0,566	0,01009	YAP1, ATF2, UPF1, MRE11, APAF1, BRCA1, SMC1A, TERF2, RASSF1, RAD50, RAD51, FANCD2, CASP3, MDM2, ABL1, NABP2, ATM, NBN	1430	55	8200	1,8767E+15	0,999	0,135	0,126
WP1530~miRNA regulation of DNA damage response	27	0,850	0,01526	RB1, CDKN1B, MRE11, BRCA1, BBC3, CCND3, CCND2, CCND1, CASP3, ABL1, NBN, APAF1, TNFRSF10B, SMC1A, PML, RAD50, RAD51, CREB1, CDK6, RRM2B, FANCD2, CDK2, CDK1, MDM2, CYCS, ATM, RAD1	1430	98	8200	1,5799E+16	1,000	0,169	0,158
WP4016~DNA IR-damage and cellular response via ATR	23	0,724	0,01869	DCLRE1A, UPF1, MRE11, UBE2D3, FANCA, HUS1, BRCA1, PPM1D, SMC1A, PML, WRN, RAD50, RAD51, RECQL5, HERC2, FANCD2, CDK2, MDM2, CDK1, RAD1, ATM, TOPBP1, NBN	1430	81	8200	1,6283E+16	1,000	0,185	0,173
WP710~DNA damage response (only ATM dependent)	28	0,881	0,03979	CDKN1B, IRS1, PTEN, PIK3R1, FOXO3, PIK3C2B, BBC3, CCND3, MAPK8, BCL2L11, CCND2, CCND1, AKT2, DVL2, ABL1, MAPK1, WNT1, LDLR, TCF7L2, WNT10B, SOD2, CCNG2, BCL2, MDM2, CTNNB1, GRB2, ATM, SOS2	1430	111	8200	1,4465E+16	1,000	0,294	0,275

Table 2.: **Genes involved in DNA repair pathways generated by the DAVID database.** After computational identification of all the potential target genes of miR-221-3p by StarBase v3.0, these were used as input information for DAVID gene enrichment analysis.

ID	Gene Name	HC
CDKN1B	cyclin dependent kinase inhibitor 1B(CDKN1B)	93
BCL2L11	BCL2 like 11(BCL2L11)	68
MDM2	MDM2 proto-oncogene(MDM2)	58
LDLR	low density lipoprotein receptor (LDLR)	39
TCF7L2	transcription factor 7 like 2(TCF7L2)	39
CASP3	caspase 3(CASP3)	38
CTNNB1	catenin beta 1(CTNNB1)	35
CCND1	cyclin D1(CCND1)	33
SMC1A	structural maintenance of chromosomes 1A(SMC1A)	30
PIK3R1	phosphoinositide-3-kinase regulatory subunit 1(PIK3R1)	29
YAP1	Yes1 associated transcriptional regulator (YAP1)	29
ATF2	activating transcription factor 2(ATF2)	27
SOD2	superoxide dismutase 2(SOD2)	22

CCND2	cyclin D2(CCND2)	18
BBC3	BCL2 binding component 3(BBC3)	17
UPF1	UPF1 RNA helicase and ATPase (UPF1)	16
CDK1	cyclin dependent kinase 1(CDK1)	15
RB1	RB transcriptional corepressor 1(RB1)	14
AKT2	AKT serine/threonine kinase 2(AKT2)	13
PTEN	phosphatase and tensin homolog (PTEN)	13
MAPK8	mitogen-activated protein kinase 8(MAPK8)	12
CDK6	cyclin dependent kinase 6(CDK6)	11
MDM4	MDM4 regulator of p53(MDM4)	11
UBE2D3	ubiquitin conjugating enzyme E2 D3(UBE2D3)	10
CCND3	cyclin D3(CCND3)	9
CREB1	cAMP responsive element binding protein 1(CREB1)	9
DVL2	dishevelled segment polarity protein 2(DVL2)	9
FANCA	FA complementation group A(FANCA)	8
PPM1D	protein phosphatase, Mg2+/Mn2+ dependent 1D(PPM1D)	8
RAD51	RAD51 recombinase (RAD51)	8
WRN	WRN RecQ like helicase (WRN)	8
APAF1	apoptotic peptidase activating factor 1(APAF1)	7
FANCD2	FA complementation group D2(FANCD2)	7
FOXO3	forkhead box O3(FOXO3)	7
MAPK1	mitogen-activated protein kinase 1(MAPK1)	7
BRCA1	BRCA1 DNA repair associated (BRCA1)	5
NBN	nibrin (NBN)	5
PIK3C2B	phosphatidylinositol-4-phosphate 3-kinase catalytic subunit type 2 beta (PIK3C2B)	5
TERF2	telomeric repeat binding factor 2(TERF2)	5
TOPBP1	DNA topoisomerase II binding protein 1(TOPBP1)	5
ABL1	ABL proto-oncogene 1, non-receptor tyrosine kinase (ABL1)	4
CCNG2	cyclin G2(CCNG2)	4
DCLRE1A	DNA cross-link repair 1A(DCLRE1A)	4
MRE11	MRE11 homolog, double strand break repair nuclease (MRE11)	4
TNFRSF10B	TNF receptor superfamily member 10b(TNFRSF10B)	4
AP3B2	adaptor related protein complex 3 subunit beta 2(AP3B2)	3
ATM	ATM serine/threonine kinase (ATM)	3
CDK2	cyclin dependent kinase 2(CDK2)	3
CYCS	cytochrome c, somatic (CYCS)	3
HERC2	HECT and RLD domain containing E3 ubiquitin protein ligase 2(HERC2)	3
RASSF1	Ras association domain family member 1(RASSF1)	3
GRB2	growth factor receptor bound protein 2(GRB2)	2
IRS1	insulin receptor substrate 1(IRS1)	2
NABP2	nucleic acid binding protein 2(NABP2)	2
PML	PML nuclear body scaffold (PML)	2
RAD1	RAD1 checkpoint DNA exonuclease (RAD1)	2
RRM2B	ribonucleotide reductase regulatory TP53 inducible subunit M2B(RRM2B)	2
BCL2	BCL2 apoptosis regulator (BCL2)	1
HUS1	HUS1 checkpoint clamp component (HUS1)	1
RAD50	RAD50 double strand break repair protein (RAD50)	1
RECQL5	RecQ like helicase 5(RECQL5)	1
SOS2	SOS Ras/Rho guanine nucleotide exchange factor 2(SOS2)	1
WNT1	Wnt family member 1(WNT1)	1
WNT10B	Wnt family member 10B(WNT10B)	1

Table 3.: **Correlation coefficient and the corresponding p-value of the miR-221-3p and the genes of interest.** Negative correlation coefficient is highlighted in red. Overlapping genes are in blue, highlighted in bold and listed in third column with their corresponding HC score and R values calculated based on the respective datasets. The calculations were performed in Matlab (Code 1.).

SW			TCGA			overlap of negative R			
GENE	R	p-value	GENE	R	p-value	GENE	HC	SW R	TCGA R
MRE11A	-0.5639	0.0004	CDKN1B	-0.2485	0.0000	BCL2L11	68	-0.2184	-0.0112
MDM4	-0.5448	0.0007	**MDM4**	-0.2432	0.0000	MDM2	58	-0.2654	-0.0812
UPF1	-0.5293	0.0011	DVL2	-0.2315	0.0000	CCND1	33	-0.1623	-0.0100
BBC3	-0.4580	0.0057	TCF7L2	-0.2288	0.0000	SMC1A	30	-0.1088	-0.0025
CDK2	-0.4559	0.0059	MAPK8	-0.2241	0.0001	ATF2	27	-0.0834	-0.1418
ABL1	-0.4380	0.0085	DCLRE1A	-0.2084	0.0002	BBC3	17	-0.4580	-0.1505
GRB2	-0.4268	0.0106	CTNNB1	-0.1888	0.0009	UPF1	16	-0.5293	-0.0822
PML	-0.4189	0.0123	**ATM**	-0.1733	0.0022	RB1	14	-0.0085	-0.1232
SOD2	-0.4171	0.0127	PPM1D	-0.1562	0.0059	MDM4	11	-0.5448	-0.2432
ATM	-0.3866	0.0218	**BBC3**	-0.1505	0.0080	FANCA	8	-0.3828	-0.1245
FANCA	-0.3828	0.0232	**ABL1**	-0.1472	0.0096	RAD51	8	-0.2095	-0.0510
TNFRSF10B	-0.3240	0.0576	NABP2	-0.1466	0.0099	APAF1	7	-0.3101	-0.1314
RASSF1	-0.3146	0.0657	**ATF2**	-0.1418	0.0126	FANCD2	7	-0.2770	-0.1163
APAF1	-0.3101	0.0699	PIK3C2B	-0.1395	0.0141	FOXO3	7	-0.0515	-0.1034
HERC2	-0.2941	0.0864	**APAF1**	-0.1314	0.0209	TOPBP1	5	-0.2625	-0.0539
FANCD2	-0.2770	0.1072	**FANCA**	-0.1245	0.0287	NBN	5	-0.2613	-0.0450
MDM2	-0.2654	0.1233	**RB1**	-0.1232	0.0304	TERF2	5	-0.2334	-0.0863
TOPBP1	-0.2625	0.1276	WRN	-0.1211	0.0333	BRCA1	5	-0.2317	-0.0953
NBN	-0.2613	0.1294	RECQL5	-0.1208	0.0338	MRE11	4	-0.5639	-0.0861
WNT10B	-0.2582	0.1343	RAD1	-0.1183	0.0377	ABL1	4	-0.4380	-0.1472
TERF2	-0.2334	0.1772	**FANCD2**	-0.1163	0.0410	CDK2	3	-0.4559	-0.0518
RRM2B	-0.2320	0.1798	PTEN	-0.1118	0.0496	ATM	3	-0.3866	-0.1733
BRCA1	-0.2317	0.1805	FOXO3	-0.1034	0.0696	HERC2	3	-0.2941	-0.0915
BCL2L11	-0.2184	0.2075	CCNG2	-0.1031	0.0702	RRM2B	2	-0.2320	-0.0493
RAD51	-0.2095	0.2271	**BRCA1**	-0.0953	0.0946	WNT10B	1	-0.2582	-0.0145
CCND1	-0.1623	0.3516	CREB1	-0.0930	0.1026	BCL2	1	-0.1583	-0.0783
BCL2	-0.1583	0.3637	**HERC2**	-0.0915	0.1083				
HUS1	-0.1492	0.3924	**TERF2**	-0.0863	0.1299				
SMC1A	-0.1088	0.5338	MRE11	-0.0861	0.1311				
ATF2	-0.0834	0.6337	**UPF1**	-0.0822	0.1493				
FOXO3A	-0.0515	0.7691	AKT2	-0.0812	0.1547				
RB1	-0.0085	0.9616	**MDM2**	-0.0812	0.1547				
CCND3	0.0140	0.9364	**BCL2**	-0.0783	0.1697				
WRN	0.0276	0.8751	RAD50	-0.0638	0.2638				
DCLRE1A	0.0344	0.8446	SOS2	-0.0587	0.3038				
RAD1	0.0497	0.7768	CYCS	-0.0560	0.3266				
CDKN1B	0.0817	0.6409	**TOPBP1**	-0.0539	0.3449				
PIK3C2B	0.0922	0.5985	**CDK2**	-0.0518	0.3637				
IRS1	0.1055	0.5464	**RAD51**	-0.0510	0.3719				
DVL2	0.1407	0.4201	**RRM2B**	-0.0493	0.3874				
YAP1	0.1415	0.4176	**NBN**	-0.0450	0.4304				
CDK6	0.1609	0.3557	AP3B2	-0.0400	0.4831				
MAPK8	0.1945	0.2628	WNT1	-0.0333	0.5598				
CASP3	0.2094	0.2273	MAPK1	-0.0260	0.6483				
CYCS	0.2095	0.2270	CASP3	-0.0184	0.7473				
CCND2	0.2193	0.2056	CCND3	-0.0167	0.7706				
PIK3R1	0.2291	0.1856	**WNT10B**	-0.0145	0.7990				

CREB1	0.2298	0.1842	PIK3R1	-0.0125	0.8266
LDLR	0.2364	0.1716	**BCL2L11**	-0.0112	0.8450
CTNNB1	0.3032	0.0767	**CCND1**	-0.0100	0.8605
PPM1D	0.3054	0.0744	**SMC1A**	-0.0025	0.9644
PTEN	0.3221	0.0592	CDK1	-0.0006	0.9910
RAD50	0.3891	0.0209	SOD2	0.0017	0.9767
UBE2D3	0.4523	0.0064	YAP1	0.0028	0.9608
RECQL5	0.4679	0.0046	HUS1	0.0050	0.9301
CCNG2	0.4828	0.0033	IRS1	0.0072	0.8997
MAPK1	0.4899	0.0028	TNFRSF10B	0.0221	0.6989
TCF7L2			GRB2	0.0301	0.5976
CDK1			CDK6	0.0613	0.2826
AKT2			LDLR	0.0660	0.2473
AP3B2			RASSF1	0.0770	0.1768
NABP2			UBE2D3	0.0848	0.1368
SOS2			CCND2	0.0947	0.0966
WNT1			PML	0.1966	0.0005

Code 1.: **Matlab code for selection of genes of interest from dataset and calculating the corresponding correlation coefficient of their co-expression with miR.** The code below is optimized for working with SW (in house) dataset. An analogous code was used for analyzing TCGA dataset.

```
Clearvars
```

find miR in the annotation table and identify ProbeName

```
tblannot_miR = readtable(,Data SW updated annotation file miRs weefsels.txt‘);
name_miR = ,miR-221‘
pos_miR = find(contains(tblannot_miR.UpdatedAnnotationMiRBaseV20,name_miR));    %find position of
miR
ProbeName_miR = tblannot_miR(pos_miR,1);                                        %find the matching
ProbeName
array_PN_miR = table2array(ProbeName_miR(:,:)                                  %save the identified
ProbeNames into an array
```

use ProbeName to find values for miRNA and calculate average values for all samples

```
tbl_miR = readtable(,microRNA microarray data cervical tissues SW.txt‘);
tbl_miRoI=table();

for i = (1:length(array_PN_miR))                    %repeat for the all the ProbeNames found
   miRoI = array_PN_miR(i);                         %choose the ith ProbeName
   pos_miRoI = find(contains(tbl_miR.Var1,miRoI));  %find position of the ProbeName in the miRNA
expression table
   tbl = tbl_miR(pos_miRoI,:;                      %save the row with the miR of interest into tbl
variable
   tbl_miRoI(i,:) = tbl;                            %put the row saved in tbl into the ith row of
tbl_miR221
end
tbl_miRoI=tbl_miRoI(:,2:end);

if height(tbl_miRoI) > 1
    AvgMiR221 = mean(tbl_miRoI{:,:});               %calculate the mean expression of miR
    tbl_avg_miR =
array2table(AvgMiR221,“VariableNames“,tbl_miRoI.Properties.VariableNames,‘RowNames‘,{name_miR})
%create a table containing the average values
else
    AvgMiR221 = table2array(tbl_miRoI);             %calculate the mean expression of miR
    tbl_avg_miR =
array2table(AvgMiR221,“VariableNames“,tbl_miRoI.Properties.VariableNames,‘RowNames‘,{name_miR})
%create a table containing the average values
end
```

find gene of interest and calculate the average values for each sample

```
tbl_genes = readtable(,mRNA microarray data cervical tissues SW.txt‘);
tbl_listGenes = readtable (,221_targets_Hcscore_SW.txt‘);
tbl_geneExp = table ();
tbl_avg_expGoI = table ();
```

```
tbl_name_GoI = table ();

for i = (1:length(tbl_listGenes.ID))
    tbl_listGenes.ID(i);
    pos_GoI = find(strcmp(tbl_genes.GeneName, tbl_listGenes.ID(i)));    %find position of GoI listed
in initial target genes list
    if length(pos_GoI) < 1
        missingGoI(1:35) = NaN
        tbl_avg_expGoI(i,:) = array2table(missingGoI)
    else
        tbl_geneExp = tbl_genes(pos_GoI,13:end);      % make a table with the values only for the
specified gene
        if height(tbl_geneExp) > 1
            Avg_ExpGoI = mean(tbl_geneExp{:,:});
            tbl_avg_expGoI(i,:) =
array2table(Avg_ExpGoI,"VariableNames",tbl_geneExp.Properties.VariableNames,"RowNames",tbl_listGenes
.ID(i));
        else
            tbl_avg_expGoI(i,:) = (tbl_geneExp);
        end
    end
    tbl_name_GoI(i,:) = tbl_listGenes.ID(i);
end

tbl_avg_expGoI.Properties.RowNames = tbl_name_GoI.Var1;
tbl_avg_expGoI.Properties.VariableNames = tbl_geneExp.Properties.VariableNames;
```

combine miRNA and genes of interest expression into one table

```
[~,order] = ismember(tbl_avg_expGoI.Properties.VariableNames, tbl_avg_miR.Properties.VariableNames);
tbl_avg_miR_ordered = tbl_avg_miR(:,order);
tbl_miR_GoI =[tbl_avg_expGoI;tbl_avg_miR_ordered];
```

calculate correlation coefficient and p-value

```
pos_miR_corr = find(contains(tbl_miR_GoI.Properties.RowNames, {name_miR}));
miR_corr = tbl_miR_GoI(pos_miR_corr,:);

for i = (1:(height(tbl_miR_GoI)-1))
    GoI_corr = tbl_miR_GoI(i,:);
    [R_GoI,p_GoI] = corrcoef(miR_corr{:,:}, GoI_corr{:,:});
    coeff = R_GoI(2);
    p_value = p_GoI(2);
    array_corr(i) = coeff;
    array_p(i) = p_value;
end

tbl_corr_p_GoI = table(array_corr',array_p');                              % make a table from the R
and p-values
tbl_corr_p_GoI.Properties.RowNames = tbl_miR_GoI.Properties.RowNames(1:height(tbl_corr_p_GoI),:);
% assign gene names to rows
tbl_corr_p_GoI.Properties.VariableNames = {,R','p-value'}                  % set variable names
tbl_corr_p_GoI_sorted = sortrows(tbl_corr_p_GoI)                           % sort the table in
ascending order of R

hm = heatmap(array_corr');
hm.Xdata = {name_miR};
hm.Ylabel = ,Genes of Interest';
hm.Colormap = jet;
hm.FontSize = 12;
hm.Ydata = (tbl_miR_GoI.Properties.RowNames(1:height(tbl_corr_p_GoI),:))';
sorty(hm,{name_miR});
```

save the R and p-value into a table

```
writetable(tbl_corr_p_GoI_sorted,'updated_SW_corr_p_GoI_sorted_221.xlsx','WriteRowNames', true)
```

Table 4.: **List of genes analyzed for expression and their qRT-PCR primers sequence.** Pairs of primers were designed to span exon-exon junction in at least one direction for each gene.

GENE	FW	RV
ATF2	CCCTCTTGCAACACCTATC	GCCAATGGTACTTCCTTCTC
BCL2L11	TCTCAGTGCAATGGCTTC	CTTCGGCTGCTTGGTAAT
CCND1	TCGTGGCCTCTAAGATGAA	TCCATTTGCAGCAGCTC
CDKN1B	TCTGAGGACACGCATTTG	GAGTAGAAGAATCGTCGGTTG
FOXO3	CCTCATCTCCACACAGAATG	AGTTTGAGGGTCTGCTTTG
MDM2	CTGTGAAAGAGCACAGGAAA	TGATCACTCCCACCTTCAA
RAD51	CGCTGATGAGTTTGGTGTAG	GATGCATGGGCGATGATATT
RB1	GGAAGCAACCCTCCTAAAC	CGTGTTCGAGTAGAAGTCATT
SMC1A	CTAGCAAGCAGTCCCTAGA	CCTGGTTCAGCTCCTTATTG
TOPBP1	CCCAGTCAGAGAAGGAAGAA	CACCTGTAATCTGCTCCTAGA
UPF1	GTCCCAGACTCAAGATAACATC	TTTGTACCGCAGGCATATC